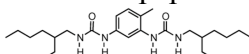**Qualifier Questions Beaucage**
Fall 2017

1) Alverenga et al. recently published a paper concerning the formation of polymer-like chains

from bis-urea EHUT which hydrogen bonds and forms a
reversible chain structure. [Alvarenga BG, Raynal M, Bouteiller L, Sabadini E
Unexpected Solvent Influence on the Rheology of Supramolecular Polymers,
Macromolecules, Article ASAP **DOI:** 10.1021/acs.macromol.7b00786 (2017)]

a) The molecular weight of this polymer-like chain would follow a distribution similar
to step-growth polymerization. **Give a function and sketch of number of chains
versus molecular weight and of mass of chains versus molecular weight.**

b) **Sketch the structure of three of these chemical units linked by hydrogen
bonds showing which groups hydrogen bond and in what orientation.
Indicate what part of the chemical structure is rigid (planar). Do you expect a
helical structure for the chain?**

c) Figure 3a shows the dynamic modulus behavior for solutions of EHUT in toluene
and in pentylbenzene. Figure 3b shows the relaxation time for various n-alkyl
benzenes and n-alkanes, (pentyl benzene is 5 and toluene is 1). **Explain how points
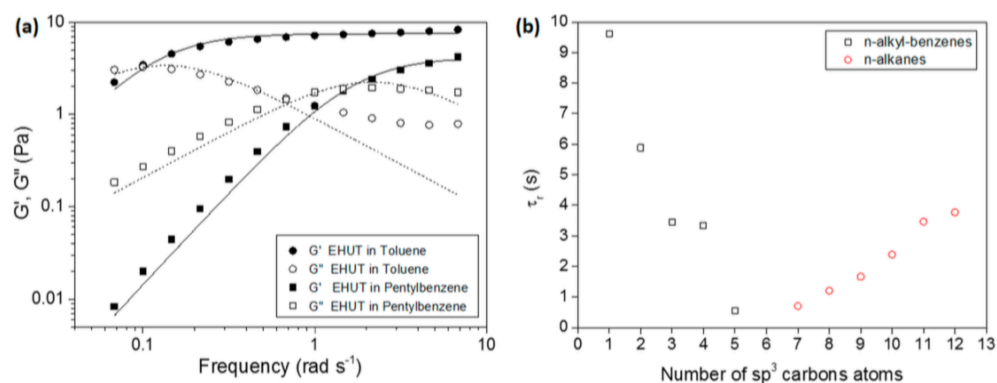1 and 5 in Figure 3b are obtained.**

Figure 3. (a) Dynamic moduli versus oscillation frequency for EHUT in toluene or pentylbenzene (6 mmol L^{-1}, 20 °C). The lines correspond to fits
with the Maxwell model. (b) Dependence of the crossover frequency for EHUT solutions in aromatic or aliphatic solvents versus the number of sp^3
carbon atoms in the solvent.

d) Figure 2 shows a similar plot of zero shear viscosity. **Explain how this plot is obtained.**
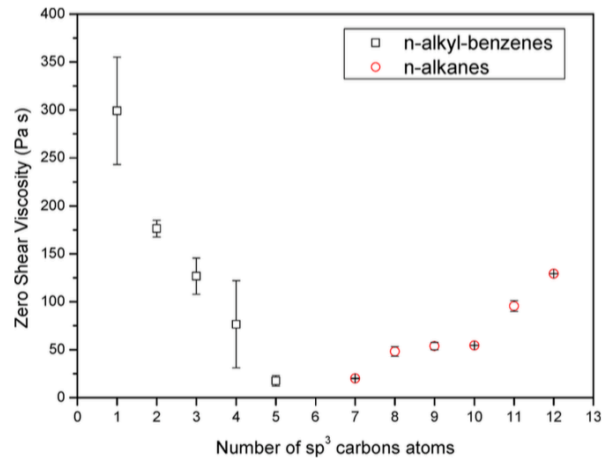

Figure 2. Dependence of the zero shear viscosity for EHUT solutions (10 mM, 20 °C) in aromatic (squares) or aliphatic (circles) solvents versus the number of sp^3 carbon atoms in the solvent (1 for toluene; 12 for dodecane).

e) Toluene displays a higher viscosity and a longer relaxation time compared to pentyl benzene as shown in the figures above, but the chains are shorter in toluene according to IR measurements. **Are these results compatible?** (Alverenga et al. use the following equation to explain this, $\tau_R = \sqrt{\tau_{rep}\tau_b}$ where τ_{rep} is the reptation time and τ_b is the chain breakage time for these weakly bound chain structures.)

2) Rabbe et al. recently published a paper on single chain polymer nanoparticles (SCPNs) [Rabbe H, Breier P, Sommer J-U, *Swelling Behavior of Single-Chain Polymer Nanoparticles: Theory and Simulation*, Macromolecules, Article ASAP **DOI:** 10.1021/acs.macromol.7b01379 (2017).] SCPNs are a biomimetic approach to the production of nanoparticles. Protein and nucleic acid chains fold to form compact native state structures through specific interactions. In SCPNs chemists design chemical crosslinks that act as structure guiding specific interactions (see graphic below).
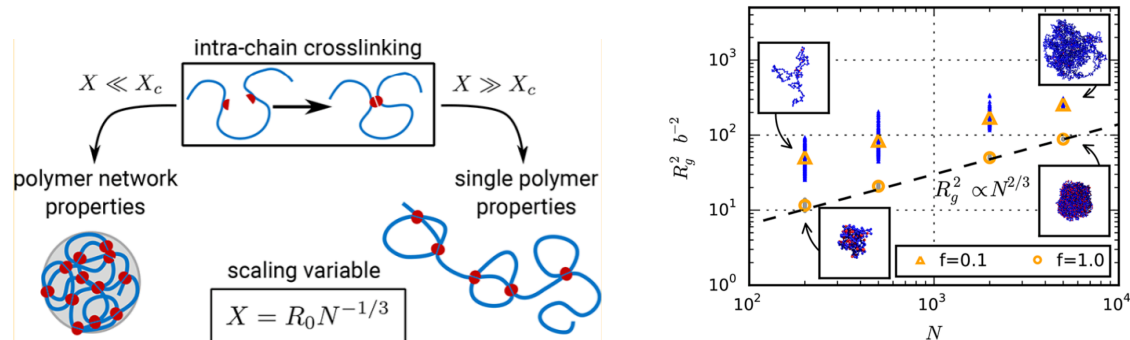

a) X in the figure is the size of the SCPN, N is the number of units in the chain. R_0 is a constant. ***Explain the structure of a nanoparticle that follows this law.***

b) Rabbe et al. propose that crosslinking in a good solvent or in a theta solvent leads to different SCPN structure. ***Explain what is meant by a good solvent and a theta solvent.***

c) ***Postulate the consequence of crosslinking under different conditions of solvation.*** For instance, how would you expect the blob model to impact this behavior? How about entanglements and other topological features such as concatenated rings?

d) It is desirable to obtain compact SCPNs since these could be effective for drug deliver or as synthetic catalysts analogous to enzymes. If a compact SCPN were formed in a theta solvent, ***explain how changes in temperature could be used for drug delivery***.

e) The second plot above shows the behavior of the average square radius of gyration as a function of the chain molar mass, N, for different $f = 4N_{act}/N$ where N_{act} are the active crosslinked units in the chain. When f = 1 the chain is linked at each monomer. When f = 0 there are no crosslinks. The plot shows simulation results for SCPNs crosslinked in a theta solvent. The triangle points **do not** display a slope of 2/3. ***Explain this plot and why it is important.***

Unexpected Solvent Influence on the Rheology of Supramolecular Polymers

Bruno G. Alvarenga,[†] Matthieu Raynal,[‡] Laurent Bouteiller,*,[‡] and Edvaldo Sabadini*,[†]

[†]Department of Physical-Chemistry, Institute of Chemistry, University of Campinas — UNICAMP, Campinas, Brazil

[‡]Sorbonne Universités, UPMC Univ Paris 06, CNRS, Institut Parisien de Chimie Moléculaire, Equipe Chimie des Polymères, 4 Place Jussieu, F-75005 Paris, France

Ⓢ *Supporting Information*

ABSTRACT: A very limited change in the nature of the solvent (toluene versus pentylbenzene) can have an unexpectedly strong effect on the viscosity of a hydrogen-bonded supramolecular polymer. In pentylbenzene, slightly stronger hydrogen bonds are formed than in toluene, but the supramolecular polymer solution is ca. 25 times *less* viscous. Several hypotheses can be envisaged to explain this counter-intuitive result. We propose that this effect is actually related to a solvation effect involving the outer corona of the supramolecular objects. When the cohesive energy density of the solvent approaches the cohesive energy density of the outer corona of the supramolecular objects, the viscosity of solution is reduced, possibly because of faster local dynamics.

toluene   *dodecane*

hydrogen bond strength

but viscosity
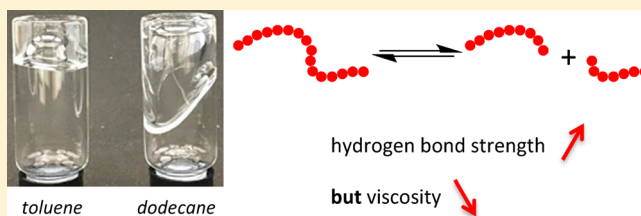
■ INTRODUCTION

The choice of the solvent has a strong influence on the outcome of any self-assembly process, which makes the rationalization of solvent effects of paramount importance. In the case of out-of-equilibrium processes such as crystal engineering,[1−3] organogelation,[4−6] or the processing of nanostructures,[7] such rationalization is particularly challenging. At first glance, the case of systems that are at thermodynamic equilibrium seems to be much better understood. For instance, in the case of hydrogen-bonded assemblies, the main solvent characteristic is known to be its polarity. The influence of the hydrogen bond competition by the solvent polar groups can even be quantitatively accounted for.[8,9] Still, when considering solvents of similar polarity, subtle effects can occur that significantly alter the outcome of the assembly structure and properties. For example, the bulkiness of aromatic solvent molecules has been shown to control the stability of tubular supramolecular assemblies because of the necessity for the solvent to fit inside the cavities.[10] Similarly, replacing a cyclic alkane solvent by a linear alkane has been shown to change the inner conformation or even the helical sense of self-assembled rods,[11−13] possibly because the thinner linear alkanes are able to intercalate between the alkyl chains of the stacked monomers. Even the length of alkane molecules has been shown to influence the stability of stacked hydrogen-bonded dimers through a strong odd−even effect.[14]

A better understanding of these and possibly other subtle solvent effects is clearly required before more complex issues such as the influence of solvent on crystal growth can be envisaged. Supramolecular polymers, i.e., long chains of noncovalently and reversibly linked repeat units, are ideal tools to study such effects because their large size can reveal

cooperative growth[15] or chiral amplification effects[16] that can conveniently be probed by spectroscopic tools and that sometimes even result in macroscopic property changes. Moreover, the absence of chain bundling avoids the complications associated with kinetic traps that can occur during the growth of other large size systems such as crystalline fibers.

The observation that a particular hydrogen-bonded supramolecular polymer (see below) forms more viscous solutions in toluene than in dodecane (see Figure 1) although dodecane is significantly less polar triggered our interest. We report here a
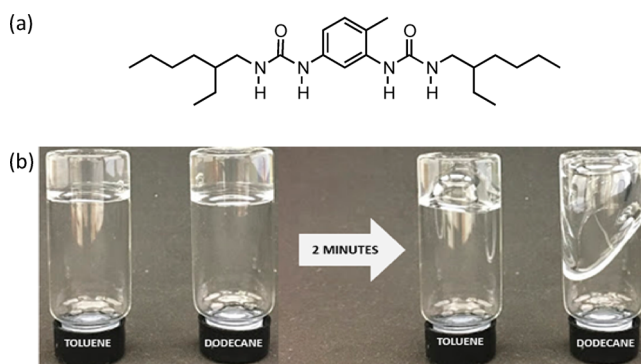
(a)

(b)

Figure 1. Structure of EHUT (a). Photographs of EHUT solutions in toluene or *n*-dodecane (b) 10 s (left) and 2 min (right) after inverting the vials (20 mmol L^{-1}, 20 °C).

careful study of this effect and show that within the family of alkylbenzene solvents an increase in the alkyl chain length leads not only to *stronger hydrogen bonds* but also to *much less viscous solutions*. We discuss possible interpretations for this highly counterintuitive effect.

■ EXPERIMENTAL SECTION

Bis-urea EHUT was synthesized as previously described.[17] All aliphatic and aromatic solvents were obtained from Sigma-Aldrich and used without purification. The amount of water (<200 ppm) in the solvents was determined by Karl Fischer analysis.

Sample Preparation. The solutions of EHUT were prepared at 80 °C in a sand bath, under stirring for at least 1 day. Then, the temperature was decreased at 5 °C/h to room temperature, and the solutions were left to rest for at least 1 day.

Rheological Measurements. Flow curves and oscillatory measurement of 6 and 10 mmol L^{-1} EHUT solutions were obtained with a Haake RheoStress 1 rheometer equipped with a Z20-din cell (volume: 8.2 mL; gap: 4.2 mm). The sample was carefully placed in the rheometer and allowed to stand for 10 min to equilibrate before measurement started. The temperature was controlled at 20.0 °C by an external water-bath system with precision better than 0.1 °C. The flow curves were obtained over a shear rate from 10^{-4} to 0.3 s^{-1}. The oscillatory experiments were carried out within linear viscoelastic range as determined through strain sweep measurements. A solvent-trap accessory was used to minimize solvent evaporation. All experiments were carried out at least in duplicate (with independent solutions). The large uncertainties for solutions in aromatic solvents (Figure 2) are possibly due to slow kinetics for reaching a homogeneous equilibrium state.
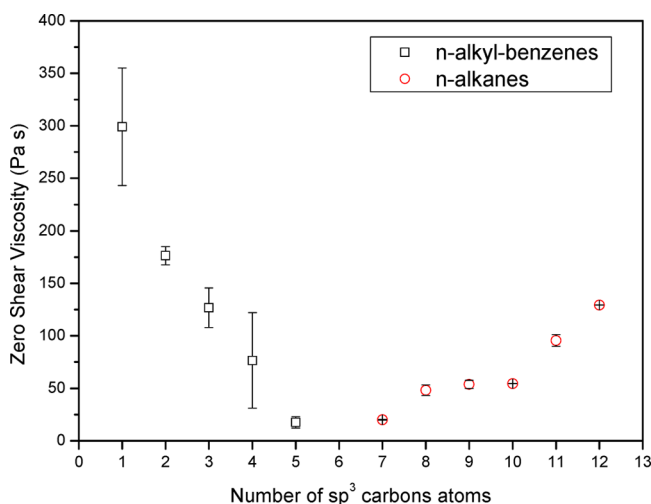

Figure 2. Dependence of the zero shear viscosity for EHUT solutions (10 mM, 20 °C) in aromatic (squares) or aliphatic (circles) solvents versus the number of sp^3 carbon atoms in the solvent (1 for toluene; 12 for dodecane).

Infrared Spectroscopy. Spectra for 1 mmol L^{-1} EHUT solutions were measured on a Nicolet iS10 spectrometer using a CaF$_2$ cell with 1 mm path length. The spectra were corrected for air, solvent, and cell absorption. The temperature was controlled with a heating device from Specac (P/N21525). Consecutive spectra were obtained separated by at least 15 min to allow thermal equilibration. Thermal expansion of solutions was not corrected.

Differential Scanning Calorimetry. Thermograms were measured using an N-DSCIII instrument from CSC. The reference cell was filled with solvent and the sample cell (0.3 mL) with 10 mmol L^{-1} EHUT solution, and a constant pressure of 5 × 10^5 Pa was applied. A baseline scan (solvent in both reference and sample cells) was performed in identical conditions and subtracted from the sample scan. The transition temperature (T^{**}) was taken as the average of heating and cooling scans, at a scan rate of 1 °C min^{-1}.

Isothermal Titration Calorimetry. The EHUT heats of dissociation were measured using a MicroCal VP-ITC titration microcalorimeter. Aliquots (5 μL) of 0.25 mmol L^{-1} EHUT solutions in a syringe were automatically injected into a continuously stirred (310 rpm) isothermal cell (1.420 cm^3) containing the pure solvent.

■ RESULTS AND DISCUSSION

Bis-urea EHUT (Figure 1) is known to self-assemble into a long hydrogen bonded tubular structure in low-polarity solvents.[18,19] Unlike some other hydrogen-bonded supramolecular polymers,[20,21] these long structures display a negligible macrodipole because both urea groups of a given monomer are oriented in an antiparallel fashion.[19] In the semidilute regime, the entanglements between these long and rigid objects (that can reversibly break and recombine) yield viscoelastic solutions. While the rheological properties of these solutions have been studied in several aliphatic or aromatic solvents,[22] the results in the various solvents have never been quantitatively compared. SANS data in dodecane and toluene indicate the supramolecular structure is the same in both solvents;[18] therefore, one expects hydrogen-bonded assemblies to be stronger in dodecane because the dielectric constant is lower in dodecane than in toluene.[23] However, the EHUT solution seems to be less viscous in dodecane than in toluene (based on the qualitative comparison of the solutions, Figure 1). In order to investigate this effect, we systematically characterized the rheology and the structure of this supramolecular polymer in a range of aliphatic and aromatic solvents.

Figure 2 shows the zero shear viscosity (obtained at the Newtonian plateau) of EHUT solutions in alkylbenzenes (toluene to pentylbenzene) and in linear alkanes (heptane to dodecane), which were obtained from the flow curves (Figures S1 and S2). In order to isolate the contribution of the solute from the solvent bulk viscosity, the zero shear viscosity of the solution (Figure 2) was normalized by the viscosity of the pure solvents (Figure S4). First of all, this data confirms the visual observation of Figure 1: the toluene solution is approximately 5 times more viscous than the dodecane one (Figure S4). Moreover, different trends are detected in aromatic and aliphatic solvents when the length of the solvent molecule is increased. The relative viscosity is roughly constant within the aliphatic series, which is expected because of the weak effect of the alkane size on the solvent properties. In particular, the polarity of the aliphatic solvents is very similar in heptane and dodecane, which means that the strength of the hydrogen bonds formed between the EHUT molecules is expected to be similar. In contrast, the relative viscosity of the solutions strongly decreases within the aromatic series: the relative viscosity is ca. 25 times lower in pentylbenzene than in toluene although the former solvent is the least polar of the series. In the following we therefore focus our attention on the aromatic solvents.

The previous viscosity measurements were complemented by oscillatory experiments in order to probe the dynamics of the supramolecular polymer. The variation of the elastic (G') and viscous (G'') moduli as a function of the frequency for solutions in toluene or pentylbenzene is shown in Figure 3 (the curves for the other solvents can be seen in Figure S5). The elastic and viscous moduli can be analyzed by considering the Maxwell model (eqs 1 and 2).
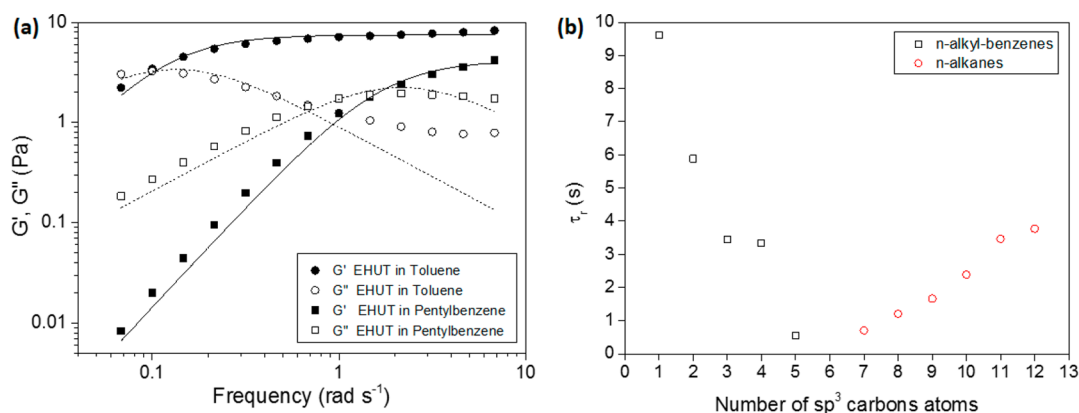
Figure 3. (a) Dynamic moduli versus oscillation frequency for EHUT in toluene or pentylbenzene (6 mmol L^{-1}, 20 °C). The lines correspond to fits with the Maxwell model. (b) Dependence of the crossover frequency for EHUT solutions in aromatic or aliphatic solvents versus the number of sp^3 carbon atoms in the solvent.

$$G'(\omega) = \frac{\omega^2 \tau_R^2}{1 + \omega^2 \tau_R^2} G_0 \tag{1}$$

$$G''(\omega) = \frac{\omega \tau_R}{1 + \omega^2 \tau_R^2} G_0 \tag{2}$$

Although the Maxwell model does not fit perfectly the curves, it can be used to discuss the results. According to this model, the dynamics of the system can be described by a single relaxation time τ_R, obtained from the crossover frequency of the two moduli ($\omega_c = 1/\tau_R$ when $G'(\omega_c) = G''(\omega_c)$).[19,24] The relaxation time measured in toluene is ca. 20 times longer than in pentylbenzene, although the plateau moduli are very similar. Moreover, the influence of the solvent on the relaxation time and on the zero shear viscosity is quantitatively very close (Figure S6). Therefore, we propose that the decrease in viscosity from toluene to pentylbenzene actually reflects acceleration of relaxation in pentylbenzene.

For chains with a reversible backbone, the shear stress can relax by two mechanisms: reptation and scission of the chains, which are described by two characteristic relaxation times: the reptation time, τ_{rep}, and the breaking time, τ_b. If the scission is much faster than the reptation ($\tau_b \ll \tau_{rep}$), the rheological behavior is perfectly described by the Maxwell model, with a single-exponential decay with a relaxation time, τ_R, given by the following expression:[25]

$$\tau_R = \sqrt{\tau_{rep} \tau_b} \tag{3}$$

Such a phenomenon was well described for gel-like solutions of wormlike micelles formed by combination of a cationic surfactant with hydrotropes such as salicylate.[26]

The high viscosity of EHUT supramolecular polymer in toluene and the associated large value of τ_R can therefore be due to a longer breaking time or to a longer reptation time (or both) in toluene than in pentylbenzene. A priori, this evolution of the relaxation times (and the viscosity) induced by the solvent could be due to a variety of reasons that we now examine.

First of all, the water content in the solvent is known to affect the viscosity of hydrogen-bonded supramolecular polymers.[27] Therefore, we checked by Karl Fischer analysis that all the solvents we used had approximately the same water content (from 80 to 200 ppm). We can therefore exclude that the

decrease in viscosity in the aromatic series is due to different water contents.

We also need to check if the structure of the supramolecular polymer is the same in the various aromatic solvents. Indeed, previous studies in toluene have shown that the tubular structure is the main supramolecular structure present at 10 mM and 20 °C but that the supramolecular tubes convert into thinner filaments at higher temperatures.[28] Since the viscosity of the filaments is lower than the one of the tubes, we have to check whether the unexpected viscosity trend is related to a possible influence of the solvent on the tube to filament equilibrium.[10] The shape of the N−H vibration band measured by FTIR spectroscopy has been shown to be characteristic of the supramolecular structure of EHUT.[18] Figure 4 shows that
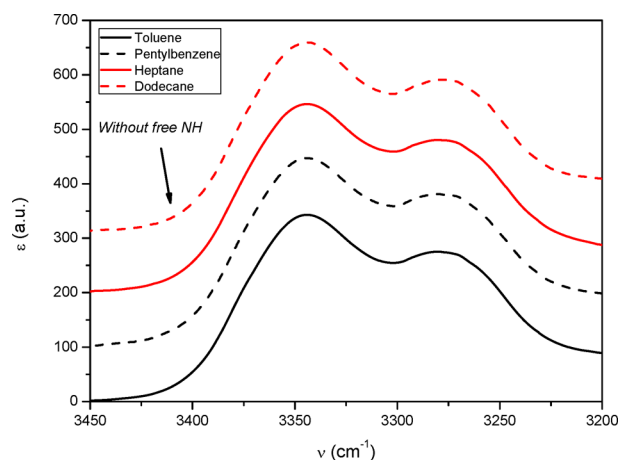

Figure 4. FTIR spectra for EHUT solutions in aromatic or aliphatic solvents (10 mmol L^{-1}, 20 °C).

the FTIR spectra in toluene and in pentylbenzene are identical and that their shape is characteristic of the tube structure. Then, the thermal stability of tube supramolecular assembly was probed both by FTIR and by DSC experiments (Figure 5). The data show that the transition temperature between tubes and filaments actually increases from toluene to pentylbenzene. The study of the phase diagram of EHUT in toluene has shown that the filament concentration is negligible at 20 °C for [EHUT] = 10 mmol L^{-1}.[28] Then, this is even more the case in pentylbenzene because of the higher tube to filament transition
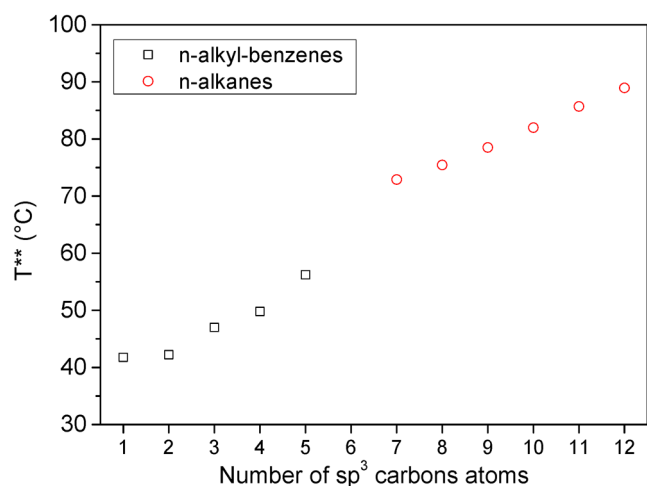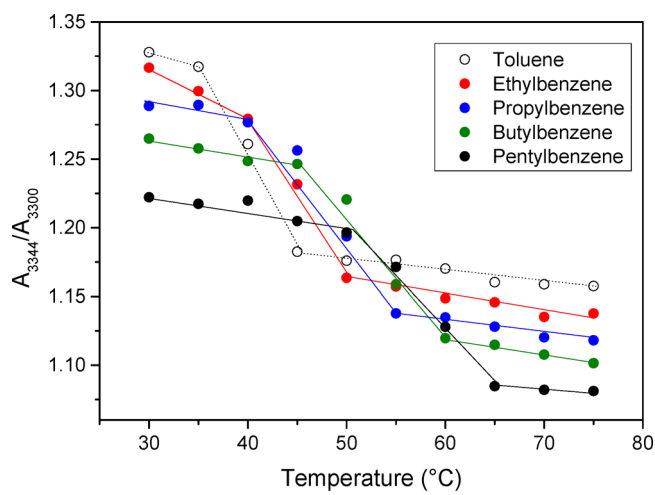
Figure 5. Transition between tube and filament structure for EHUT solutions in aromatic solvents, measured by (a) the shape of the FTIR band (1 mmol L^{-1}) or (b) DSC (10 mmol L^{-1}).

In order to see if a change in length of the assemblies could be a relevant explanation, FTIR spectroscopy was used to qualitatively probe the strength of hydrogen bonds in these solvents. Figure 4 shows that EHUT is fully hydrogen bonded in both solvents (at 10 mM and 20 °C); i.e., no free N−H vibration band is detected. In order to favor dissociation of the assemblies, the concentration was reduced to 1 mM and the temperature was increased. Figure 6 shows that at 75 °C a small contribution of free N−H groups can be detected in toluene, but not in pentylbenzene. Although at this temperature the main assembly in both solvents is not the tube (but the filament), this experiment confirms the expectation that the hydrogen bonds are stronger in pentylbenzene than in toluene because of the lower dielectric constant of the former solvent (see Figure S7).

In an attempt to obtain more quantitative information about the self-assembly process, isothermal titration calorimetry (ITC) was used. Figure 7 shows the enthalpograms obtained
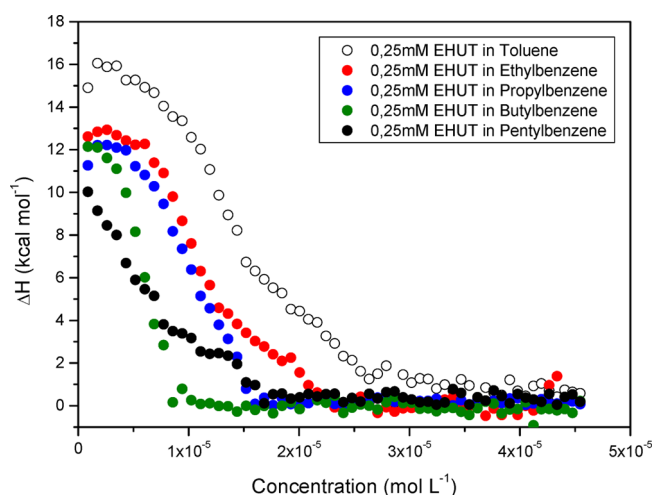

Figure 7. ITC enthalpograms for 0.25 mmol L^{-1} EHUT solutions in aromatic solvents injected into the same pure solvent (25 °C).

when a 0.25 mmol L^{-1} EHUT solution is injected into the corresponding pure solvent at 25 °C. The endothermal heat effects detected are proportional to the amount of hydrogen bonds broken during the dilution. The fact that the heat effects are smaller and shifted to lower concentrations in the case of pentylbenzene means that the assemblies are stronger (i.e., more difficult to break) in this solvent.[30] Unfortunately, the

temperature in this solvent. Therefore, it is safe to consider that the tube supramolecular structure is the only type of assembly present at the temperature and concentrations of the rheological experiments of Figures 2 and 3; i.e., the evolution of viscosity in the aromatic solvents is not due to a change in supramolecular structure.[29]
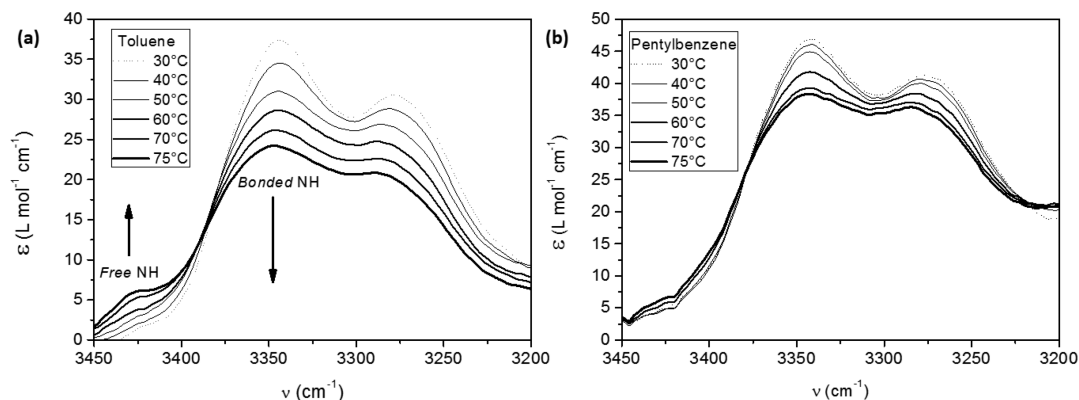

Figure 6. FTIR spectra for EHUT solutions in toluene (a) or pentylbenzene (b) (1 mmol L^{-1}).

data did not allow a consistent fit that would have yielded the thermodynamic parameters for the supramolecular polymerization in pentylbenzene. Still the ITC and FTIR data both indicate qualitatively a stronger hydrogen bonding in pentylbenzene than in toluene, which probably means that the supramolecular polymers are longer in pentylbenzene.[31] Therefore, the solvent effect on the length of the assemblies can probably not explain the lower viscosity in pentylbenzene. However, at this point it is not possible to rule out an influence of the solvent on the length dispersity of the chains. A quantitative fit of the ITC data would be required to conclude on this point.

If the faster macroscopic dynamics measured by rheology in pentylbenzene is not due to shorter chains,[32] it has to be due to faster local dynamics, i.e., to faster scission and recombination of the tubes in pentylbenzene than in toluene. The independent influence of dynamics and thermodynamics has actually been unambiguously exemplified by Craig et al. with metal–ligand systems.[34] In our case, the reason why the hydrogen-bonded tubes (that are more stable in pentylbenzene) would nevertheless break and recombine faster than in toluene is not immediately obvious. However, the reason may be related to a subtle solvation effect. Indeed, the cohesive energy density of the solvent, measured by the Hildebrand solubility parameter, decreases significantly from 18.2 MPa$^{1/2}$ for toluene to 17.4 MPa$^{1/2}$ for pentylbenzene.[35] Therefore, the 2-ethylhexyl chains of EHUT (16 MPa$^{1/2}$) that form a corona around the nanotube are better solvated in pentylbenzene than they are in toluene. Moreover, the scission of a tube in two parts involves the formation of two new ends that necessitate new solvation shells. We propose that the creation of these additional solvation shells is a faster process in a solvent (pentylbenzene) that better solvates the 2-ethylhexyl corona.

Alternatively, a possible consequence of the better solvation of the 2-ethylhexyl corona in pentylbenzene is that tube–tube contacts that occur at entanglement points could relax faster than in toluene, therefore accelerating the dynamics of tube–tube interactions. At this point, we cannot discriminate between an intratube effect (i.e., faster scission and recombination) or an intertube effect (i.e., faster disentanglement), but the parallel evolution of the overall dynamics and of the cohesive energy density point toward the strong influence of solvation.

CONCLUSION

In conclusion, we report that a very limited change in the nature of the solvent can have a strong effect on the viscosity of a hydrogen-bonded supramolecular polymer. To our best knowledge, this is the first example where slightly *stronger* hydrogen bonding actually leads to much *less viscous* solutions. We propose that this effect is actually related to a solvation effect involving the outer corona of the supramolecular objects. When the cohesive energy density of the solvent approaches the cohesive energy density of the outer corona of the supramolecular objects, the viscosity of the solution is reduced, possibly because of faster local dynamics. Further work is needed to assess the possibility of tuning the dynamics of a supramolecular polymer by changing the nature of the solvent.

ASSOCIATED CONTENT

ⓢ Supporting Information

The Supporting Information is available free of charge on the ACS Publications website at DOI: 10.1021/acs.macromol.7b00786.

Additional rheology data (PDF)

AUTHOR INFORMATION

Corresponding Authors
*E-mail sabadini@iqm.unicamp.br (E.S.).
*E-mail laurent.bouteiller@upmc.fr (L.B.).

ORCID 🔵
Matthieu Raynal: 0000-0001-6830-1668
Laurent Bouteiller: 0000-0001-7613-7028

Notes
The authors declare no competing financial interest.

REFERENCES

(1) Goesten, M. G.; Kapteijn, F.; Gascon, J. Fascinating Chemistry or Frustrating Unpredictability: Observations in Crystal Engineering of Metal-Organic Frameworks. *CrystEngComm* **2013**, *15*, 9249–9257.

(2) Blagden, N.; Berry, D. J.; Parkin, A.; Javed, H.; Ibrahim, A.; Gavan, P. T.; De Matos, L. L.; Seaton, C. C. Current Directions in Co-Crystal Growth. *New J. Chem.* **2008**, *32*, 1659–1672.

(3) Lovette, M. A.; Browning, A. R.; Griffin, D. W.; Sizemore, J. P.; Snyder, R. C.; Doherty, M. F. Crystal Shape Engineering. *Ind. Eng. Chem. Res.* **2008**, *47*, 9812–9833.

(4) Lan, Y.; Corradini, M. G.; Weiss, R. G.; Raghavan, S. R.; Rogers, M. A. To Gel or Not to Gel: Correlating Molecular Gelation with Solvent Parameters. *Chem. Soc. Rev.* **2015**, *44*, 6035–6058.

(5) Bonnet, J.; Suissa, G.; Raynal, M.; Bouteiller, L. Organogel Formation Rationalized by Hansen Solubility Parameters: Dos and Don'ts. *Soft Matter* **2014**, *10*, 3154–3160.

(6) Dasgupta, D.; Guenet, J.-M. The Solvent in Physical Gelation: Polymers Versus Organogelators. *Macromol. Chem. Phys.* **2013**, *214*, 1885–1892.

(7) Chen, Y.; Zhan, C.; Yao, J. Understanding Solvent Manipulation of Morphology in Bulk-Heterojunction Organic Solar Cells. *Chem. - Asian J.* **2016**, *11*, 2620–2632.

(8) Cook, J. L.; Hunter, C. A.; Low, C. M. R.; Perez-Velasco, A.; Vinter, J. G. Solvent Effects on Hydrogen Bonding. *Angew. Chem., Int. Ed.* **2007**, *46*, 3706–3709.

(9) Amenta, V.; Cook, J. L.; Hunter, C. A.; Low, C. M. R.; Sun, H.; Vinter, J. G. Interplay of Self-Association and Solvation in Polar Liquids. *J. Am. Chem. Soc.* **2013**, *135*, 12091–12100.

(10) Pinault, T.; Isare, B.; Bouteiller, L. Solvents with Similar Bulk Properties Induce Distinct Supramolecular Architectures. *ChemPhysChem* **2006**, *7*, 816–819.

(11) Cantekin, S.; Nakano, Y.; Everts, J. C.; van der Schoot, P.; Meijer, E. W.; Palmans, A. R. A. A Stereoselectively Deuterated Supramolecular Motif to Probe the Role of Solvent during Self-Assembly Processes. *Chem. Commun.* **2012**, *48*, 3803–3805.

(12) Nakano, Y.; Hirose, T.; Stals, P. J. M.; Meijer, E. W.; Palmans, A. R. A. Conformational Analysis of Supramolecular Polymerization Processes of Disc-like Molecules. *Chem. Sci.* **2012**, *3*, 148–155.

(13) Nakano, Y.; Markvoort, A. J.; Cantekin, S.; Filot, I. A. W.; ten Eikelder, H. M. M.; Meijer, E. W.; Palmans, A. R. A. Conformational Analysis of Chiral Supramolecular Aggregates: Modeling the Subtle Difference between Hydrogen and Deuterium. *J. Am. Chem. Soc.* **2013**, *135*, 16497–16506.

(14) Jonkheijm, P.; van der Schoot, P.; Schenning, A. P. H. J.; Meijer, E. W. Probing the Solvent-Assisted Nucleation Pathway in Chemical Self-Assembly. *Science* **2006**, *313*, 80–83.

(15) De Greef, T. F. A.; Smulders, M. M. J.; Wolffs, M.; Schenning, A. P. H. J.; Sijbesma, R. P.; Meijer, E. W. Supramolecular Polymerization. *Chem. Rev.* **2009**, *109*, 5687−5754.

(16) Palmans, A. R. A.; Meijer, E. W. Amplification of Chirality in Dynamic Supramolecular Aggregates. *Angew. Chem., Int. Ed.* **2007**, *46*, 8948−8968.

(17) Lortie, F.; Boileau, S.; Bouteiller, L.; Chassenieux, C.; Deme, B.; Ducouret, G.; Jalabert, M.; Laupretre, F.; Terech, P. Structural and Rheological Study of a Bis-Urea Based Reversible Polymer in an Apolar Solvent. *Langmuir* **2002**, *18*, 7218−7222.

(18) Bouteiller, L.; Colombani, O.; Lortie, F.; Terech, P. Thickness Transition of a Rigid Supramolecular Polymer. *J. Am. Chem. Soc.* **2005**, *127*, 8893−8898.

(19) Shikata, T.; Nishida, T.; Isare, B.; Linares, M.; Lazzaroni, R.; Bouteiller, L. Structure and Dynamics of a Bisurea-Based Supramolecular Polymer in N-Dodecane. *J. Phys. Chem. B* **2008**, *112*, 8459−8465.

(20) Sakamoto, A.; Ogata, D.; Shikata, T.; Urakawa, O.; Hanabusa, K. Large Macro-dipoles Generated in a Supramolecular Polymer of N,N′,N″-tris(3,7-dimethyloctyl)benzene-1,3,5-tricarboxamide in n-decane. *Polymer* **2006**, *47*, 956−960.

(21) Swiergiel, J.; Bouteiller, L.; Jadzyn, J. Hierarchical Structure of Supramolecular Polymers Formed by N,N′-Di(2-Ethylhexyl)Urea in Solutions. *J. Phys. Chem. B* **2015**, *119*, 12947−12953.

(22) Isare, B.; Pensec, S.; Raynal, M.; Bouteiller, L. Bisurea-Based Supramolecular Polymers: From Structure to Properties. *C. R. Chim.* **2016**, *19*, 148−156.

(23) Abed, S.; Boileau, S.; Bouteiller, L. Supramolecular Association of Acid-Terminated Poly(dimethylsiloxane)s. 2. Molecular Weight Distributions. *Macromolecules* **2000**, *33*, 8479−8487.

(24) Francisco, K. R.; Dreiss, C. A.; Bouteiller, L.; Sabadini, E. Tuning the Viscoelastic Properties of Bis(urea)-Based Supramolecular Polymer Solutions by Adding Cosolutes. *Langmuir* **2012**, *28*, 14531−14539.

(25) Cates, M. E. Reptation of Living Polymers: Dynamics of Entangled Polymers in the Presence of Reversible Chain-Scission Reactions. *Macromolecules* **1987**, *20*, 2289−2296.

(26) Rehage, H.; Hoffmann, H. Rheological Properties of Viscoelastic Surfactant Systems. *J. Phys. Chem.* **1988**, *92*, 4712−4719.

(27) Louhichi, A.; Jacob, A. R.; Bouteiller, L.; Vlassopoulos, D. Humidity affects the viscoelastic properties of supramolecular living polymers. *J. Rheol.* **2017**, in press. DOI: http://dx.doi.org/10.1122/1.4997600.

(28) Bellot, M.; Bouteiller, L. Thermodynamic Description of Bis-Urea Self-Assembly: Competition between Two Supramolecular Polymers. *Langmuir* **2008**, *24*, 14176−14182.

(29) The fact that the transition enthalpies are similar in all the aromatic solvents (ca. 1 kcal/mol) is also consistent with the formation of the same supramolecular structure.

(30) Arnaud, A.; Bouteiller, L. Isothermal Titration Calorimetry of Supramolecular Polymers. *Langmuir* **2004**, *20*, 6858−6863.

(31) In the case of an isodesmic growth, stronger binding means a larger association constant, which implies longer chains. However, in the case of a cooperative growth, it is mathematically possible that larger association constants actually lead to shorter chains if the cooperativity is weaker. Unfortunately, the ITC data in pentylbenzene do not allow a quantitative fit of the data that could settle this point.

(32) Branching has been found to be responsible for faster relaxation of wormlike micelles.[33] However, it is difficult to imagine a hydrogen-bonded structure for the bis-urea that would lead to branching.

(33) Khatory, A.; Lequeux, F.; Kern, F.; Candau, S. J. Linear and Nonlinear Viscoelasticity of Semidilute Solutions of Wormlike Micelles at High Salt Content. *Langmuir* **1993**, *9*, 1456−1464.

(34) Yount, W. C.; Loveless, D. M.; Craig, S. L. Small-Molecule Dynamics and Mechanisms Underlying the Macroscopic Mechanical Properties of Coordinatively Cross-Linked Polymer Networks. *J. Am. Chem. Soc.* **2005**, *127*, 14488−14496.

(35) Hansen, C. M., Ed.; *Hansen Solubility Parameters: A User's Handbook*; CRC Press LLC: 2007.

Swelling Behavior of Single-Chain Polymer Nanoparticles: Theory and Simulation

Hauke Rabbel,[†] Patrick Breier,[†] and Jens-Uwe Sommer*,[†,‡]

[†]Leibniz-Institut für Polymerforschung Dresden e.V., Hohe Str. 6, 01069 Dresden, Germany

[‡]Institute of Theoretical Physics, Technische Universität Dresden, Zellescher Weg 17, 01069 Dresden, Germany

ABSTRACT: Cross-linking a single polymer chain with itself leads to soft nanoparticles with well-defined properties. We study such single-chain nanoparticles (SCNP) obtained by cross-linking in good and in poor solvents using Monte Carlo simulations and theoretical models. We show that SCNP obtained by cross-linking in poor solvents preserve their shape during swelling in good solvents only if the precursor chain is very long. In this case the Flory–Rehner model describes the swelling of SCNP. Shorter chains and SCNPs cross-linked in good solvent generate noncompact structures. Here we obtain a good theoretical description of the simulated swelling properties using a mean-field model by taking into account the cross-linking topology using the connectivity matrix of the cross-linked chain. The crossover between the two regimes can consistently be described using a scaling argument. We further show that the distances between cross-links along the chain contour follows the distribution for Gaussian chains after cross-linking under poor solvent conditions.
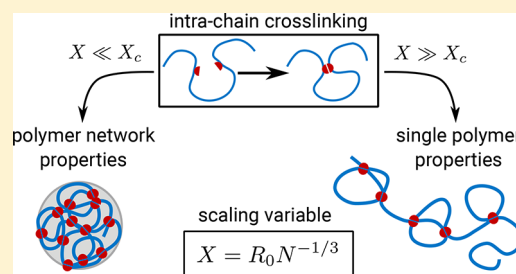
1. INTRODUCTION

Single-chain nanoparticles (SCNPs) are polymeric objects consisting of a single polymer chain, which is folded back onto itself and compactified by the formation of intramolecular cross-links (Figure 1). This concept was first demonstrated by
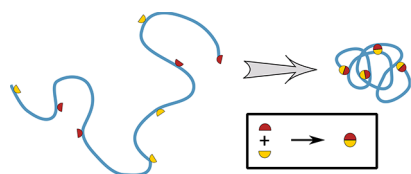

Figure 1. Concept of single chain folding into internally cross-linked nanoparticles.

Mercerreyes and co-workers[1] and is to date receiving a considerable amount of interest in polymer science.[2−4] Taking inspiration from the complex folded structures of proteins and other biomolecules,[5] as well as the expectation that synthetic polymers can be equipped with useful functionalities, single chain objects with a number of different shapes such as globules, tadpoles, or hairpins have been synthesized, as summarized in a recent review.[6]

Even though the field is still comparatively young, a promising variety of possible applications of SCNPs have been brought up. For example, SCNP-based formulations have been demonstrated to function as drug delivery systems facilitating rapid cellular uptake of peptides,[7] exhibit controlled, pH-dependent release of encapsuled cargos,[8] or could be functionalized to show catalytic, enzyme-mimetic properties.[9−11] Another suggested application is the use as agents for tuning the rheological properties of polymeric com-

pounds.[12] The examples given here are anything but exhaustive, and more complete overviews can be found in the reviews cited above.

The available strategies of fabrication and synthesis of SCNPs have also seen significant development in recent years. Possible routes of synthesis include covalent cross-linking, for example, by heat-[13] or light-induced[14−16] reactions or "click" chemistry.[17] Other options are dynamic-covalent reactions,[18] or noncovalent chemistry,[19,20] which provide the possibility of creating smart nanoparticles featuring conformational changes under different environmental conditions. A good overview including new advances is provided in recent reviews.[3,4]

This being said, the field still faces a number of big challenges[2] apart from the search for strategies to achieve controlled folding of the polymer chains. A solid theoretical understanding of the properties and microstructure of SCNPs is only beginning to emerge. To this date, only a handful of simulation studies have been published on this matter. A group of authors have published a series of papers presenting results of coarse-grained molecular dynamics simulations combined with experimental studies.[21−24] One of their central messages is that single chains, folded to SCNPs under good solvent conditions, do not form compact globular structures in the sense of the radius of gyration R_g scaling with the degree of polymerization N as $R_g \propto N^{1/3}$. This result is backed by evidence provided by other groups, which can be seen clearly in a recently published literature survey.[25] Different strategies have been suggested for obtaining more compact globules from

A

single chain folding. Among them are the use of of multifunctional cross-linkers and relatively long reactive side chains[23] and with particular success also cross-linking under poor solvent conditions.[24] Another approach is orthogonal folding,[21,22,26] i.e., the use of a number of different reactive cross-linkers on a polymer, which can react exclusively with other cross-linkers of the same type.

The most fascinating theoretical aspect of SCNPs is that their structure is in between a single polymer and a polymer network. By increasing the length of the linear precursor and the number of cross-links, a transition from a fluffy rather branched structure to a nanogel is expected. The properties of the latter are then determined by the elasticity of the strands between the cross-links. One of the challenges of theoretical polymer physics in this context is the development of analytical models for the SCNP properties and identification of the essential parameters which control in particular the crossover between different macroscopic states.

In this work we present results of generic Monte Carlo simulations of SCNPs. We analyze the network structure formed in the random cross-linking process with irreversible cross-links and demonstrate that a Flory-like theory can be successfully used to link the microstructure of SCNPs with their radius of gyration. This works for structures cross-linked under good and poor solvent conditions. We furthermore investigate as to how far the swelling of these nanonetworks in good solvent can be described by the Flory−Rehner theory for macroscopic polymer networks.

2. METHODS

We use the bond fluctuation model[27,28] (BFM) for our simulations. In this generic, coarse-grained model, monomers are represented by cubes on a simple cubic lattice, which are not allowed to overlap (excluded volume condition). Bonds between monomers are modeled by allowing only a restricted set of relative distance vectors between connected monomers. For the collapse of the polymer chains under poor solvent conditions we use an explicit repulsive solvent. Solvent molecules are modeled as single, unconnected monomers which interact with the polymer chain through a nearest-neighbor contact interaction. Each contact between a solvent monomer and the polymer is attributed with an energy penalty of $\epsilon = 0.8 k_B T$. This model has previously been successfully used to model polymers under varying solvent conditions.[29,30]

The formation and swelling of SCNPs was realized as a three-step simulation procedure (Figure 2). The first step was generation and collapse of the polymer in the solvent. A polymer chain was generated randomly in the simulation box using a self-avoiding walk algorithm. Four different polymer lengths of $N = 200-5000$ were used. The box dimensions were $(256a)^3$ for chains with $N \leq 500$ and $(512a)^3$ otherwise. Here, a is the lattice spacing of the underlying simple cubic lattice. The box was then filled with explicit solvent up to a total volume occupation of 0.5. The subsequent simulation, in which the polymer coil collapsed into a globule, was carried out using a GPU accelerated algorithm recently published by our group.[30] This procedure took 2×10^7 Monte Carlo sweeps (MCS) for the longest chains. In the second step the cross-linking procedure was carried out. For this purpose we first marked every second monomer along the polymer chain as potentially reactive. The remaining monomers were not allowed to form any new bonds during the simulation. This ensures that bond formation between neighboring monomers
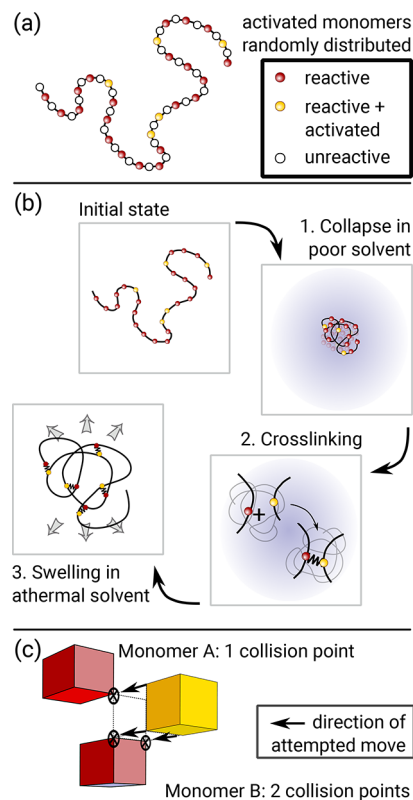

Figure 2. Schematic representation of simulation procedure used for cross-linking. (a) A random realization of a linear chain is constructed by making every second monomer reactive and randomly selecting a fraction of them to be activated. (b) The chains are collapsed to compact globules in poor solvent and swollen under athermal solvent conditions after cross-linking. (c) Cross-linking is realized whenever an unreacted, activated monomer collides with reactive monomers. In the case of multiple options for a reaction, the reaction partner is randomly chosen, weighted by the number of collision points.

along the chain is automatically exluded in the cross-linking procedure. Then, out of the $N/2$ reactive sites, where N is the overall number of monomers in the chain, a number of N_{act} monomers were randomly selected as being "activated". These N_{act} monomers can then form bonds with the remaining $N/2 - N_{act}$ reactive sites. Thus, a maximum number of $N/4$ bonds could be formed during the simulation, if half of the reactive sites were activated. The formation of the bonds itself was realized by the following procedure: The BFM simulation scheme was carried out normally; i.e., monomers were moved at random by a single step on the lattice, and moves were rejected in the case of a collision. Whenever such a collision occurred between an unreacted, activated monomer, and an unreacted reactive site, a bond was formed with a probability p. For all data shown in this article, we set $p = 1.0$. If, in a single move, a collision with more than one reactive site occurred, the bond partner was chosen at random, weighted by the number of colliding corners. This procedure is illustrated in Figure 2. After all activated sites have formed bonds, we call the ratio

$$f = 4N_{act}/N$$

the cross-linking density, such that $f \in [0, 1]$. It took only a few ten thousand Monte Carlo sweeps for nearly all activated sites to react. For high cross-linking densities not all possible reactions actually occurred before cross-linking was stopped after 2×10^5 MCS. At $f = 0.9$ the extent of reaction was on

average 97%, while it reached only 90−94% at f = 1.0. For all other cross-linking densities more than 99% of the possible reactions always occurred. After the cross-linking step, the third part of the simulation procedure was swelling the cross-linked SCNPs under athermal solvent conditions. For this purpose the explicit solvent was removed from the simulation box, and the cross-linked structure was simulated for between 2×10^7 MCS for the shortest chains at high f and 2×10^9 MCS for the longest chains at low f. This was sufficient for the structures to swell to the equilibrium size and allow for a calculation of average properties. All simulation steps after the initial collapse of the chain were carried out on CPUs, as they are less computationally demanding.

For each set of parameters N, f between 50 and 250 independent realizations of the molecular structure were simulated following the procedure described above. Generally, a higher number of realizations was chosen with decreasing f, such that also for low numbers of bonds good statistics regarding the distribution of bonds along the chain could be achieved. For N = 5000 the number of independent realizations was reduced to between 20 and 100.

For comparison, we also simulated the formation of SCNPs under athermal solvent conditions, i.e., using implicit solvent. Instead of the first step described above (the coil−globule collapse), the chains were in this case equilibrated for approximately one Rouse time τ_R, before the cross-linking procedure was started. The number of independently simulated structures was 25 for N = 5000 and every value of f, and it was 100 for all other chain lengths. Because of the less dense conformations in this setup, it took a lot longer for the activated monomers to react as compared to the cross-linking from the globular state. Here, 3×10^8 MCS were required for almost all reactions to occur for the longest chains, and even for the highest cross-linking densities the extent of reaction reached more than 98% for all chain lengths.

3. RESULTS AND DISCUSSION

3.1. Scaling Behavior. As a first characterization of the structure, we examine the scaling of the radius of gyration of SCNPs with the chain length N. For this purpose we determine the scaling exponents $\langle R_g^2 \rangle \propto N^{2\nu}$ as a function of the cross-linking density f for SCNPs constructed under both good and poor solvent conditions. Here, $\langle R_g^2 \rangle$ denotes the ensemble average, i.e., the radius of gyration averaged over different random structures at given f. The results are shown in Figure 3. It is evident that even for high cross-linking densities the SCNPs obtained from cross-linking in good solvent do not form dense globules. We observe exponents in the range $\nu \approx$ 0.5−0.6, indicating a linear structure. On the other hand, SCNPs formed in poor solvent, and swollen under good solvent conditions, appear to stay in a globular state even for the lowest values of f > 0 used here, as indicated by scaling exponents of $\nu \approx$ 0.3. The marked difference between structures obtained under different solvent conditions is a consequence of bonds predominantly forming between monomers which are close along the chain in good solvent. This is different in poor solvent, as analyzed in more detail in section 3.4. Our observations are in accordance with results from other groups.[24,25] We note that employing sequential or multiorthogonal cross-linking protocols can improve the compactification of SCNPs, but these approaches do not overcome the general limitations of cross-linking linear chains under good solvent conditions.[21,22] Figure 4 shows representa-
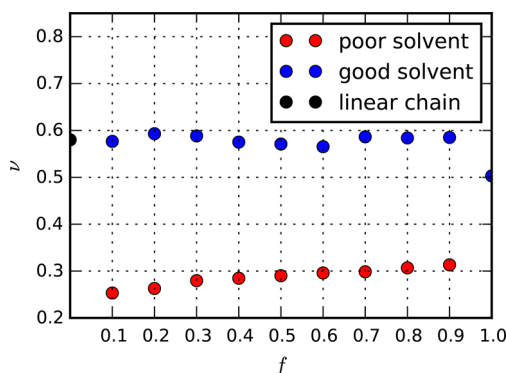

Figure 3. Scaling exponents obtained for the ensemble average radius of gyration $\langle R_g^2 \rangle \propto N^{2\nu}$ of SCNPs obtained under good and poor solvent conditions as a function of the cross-linking density f. Exponents close to $\nu \approx 0.3$ indicate a compact, globular shape. At low f in the poor solvent case the exponents become smaller than 0.3 because short chains under these conditions do not lead to compact globules (see also Figure 5 and the analysis in section 3.3).

tive simulation snapshots of structures with N = 2000, obtained under different solvent conditions and cross-linking densities.
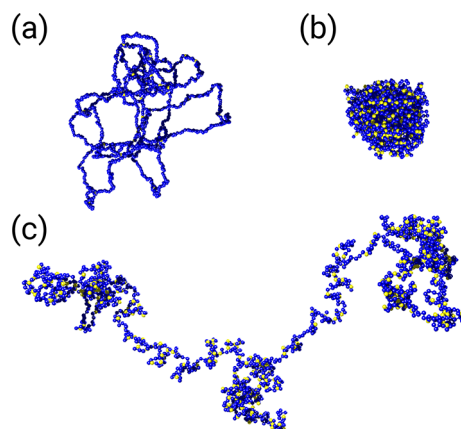

Figure 4. Simulation snapshots of SCNPs as obtained from linear chains with N = 2000 monomers. (a) and (b) were obtained using cross-linking in poor solvent with cross-linking desities f = 0.1 and f = 0.8, respectively. The snapshots show the structures after swelling in good solvent. (c) is an example of a noncompact structure obtained from cross-linking in good solvent with f = 0.8. The yellow beads in the snapshots represent the activated cross-linkers.

Notably, the exponents obtained for cross-linking under poor solvent show a clear trend to lower values with decreasing f > 0, with resulting exponents significantly below ν = 0.33, the exponent for compact globules. Even though such low values have been reported by others,[24] the observed trend raises the question for the reason behind this unexpected behavior. As it turns out, the origin is found in the fact that it is not the cross-linking density f alone that determines whether or not the chain stays folded in a globular shape. This can be understood based on the data presented in Figure 5. There, the radius of gyration R_g^2 is shown as a function of N for structures with two different cross-linking densities f = 0.1 and f = 1.0, along with a few representative simulation snapshots. It can be seen clearly that cross-linked chains with N = 5000 remain in a globular state after swelling even at f = 0.1. Opposed to that short chains with N = 200 are globular at high f = 1.0 but unfold to a spacially
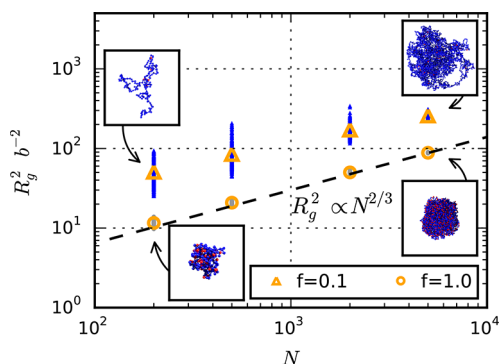
Figure 5. Square radius of gyration of polymers cross-linked under poor solvent conditions at two different cross-linking densities. The small symbols represent results from all random realizations, while the larger symbols are the averages. The inset snapshots show structures close to the average $\langle R_g^2 \rangle$ as a representative example. At $f = 1.0$ the swollen structures remain globular for all N. Opposed to this, the polymers are globular only for high N at $f = 0.1$, while they unfold into open structures for low N. This leads to reduced apparent scaling exponents $\langle R_g^2 \rangle \propto N^{2\nu}$ for low f.

extended structure with only a few loops at $f = 0.1$. Directly calculating the scaling exponents ν by fitting $\langle R_g^2 \rangle$ at constant f thus leads to an underestimation of ν with the consequence that the exponents potentially misrepresent the conformational properties. This can be considered as a particular finite-size effect for SCNPs and is analyzed further in section 3.3 in terms of a mean-field model and scaling arguments.

3.2. Flory−Rehner Theory. Here we examine as to how far the swelling of SCNPs formed under poor solvent conditions can be described by the Flory−Rehner theory for polymer networks. The main idea of the Flory−Rehner theory is that an elastic contribution to the free energy, F_{el}, is counterbalanced by a contribution F_{ev} due to the excluded volume interactions between the monomers in the network:

$$F = F_{el} + F_{ev} = \frac{3}{2}\gamma M Q^{2/3} + \nu \frac{N^2}{V}$$
$$= \frac{3}{2}\gamma M Q^{2/3} + \frac{\nu}{\nu_0} \frac{M N_S}{Q} \tag{1}$$

where F is given in units of $k_B T$. Here, M is the number of network strands contributing equally to the elastic term, N_S is the (average) length of a strand defined by N/M, and γ is a numerical constant indicating the fraction of elastic active strands. Further, ν denotes the excluded volume constant, ν_0 is the eigenvolume of a segment in the melt state, and V is the volume of the swollen network. The volume swelling ratio is defined as

$$Q = V/V_0 \propto R_g^3/R_0^3 \tag{2}$$

where V_0 is the reference volume of the network with the corresponding radius of gyration R_0. In our case we have $V_0 = \nu_0 N$ because we start from a compact globular state. Minimizing eq 1 with respect to Q gives the equilibrium degree of swelling

$$Q_{eq} = \left(\frac{\nu}{\nu_0 \gamma} N_S \right)^{3/5}$$

The average strand length N_S and can be expressed by the cross-linking density, giving in our definition $N_S = 2/f$.

Furthermore, to obtain an expression for the equilibrium radius of gyration, we can use eq 2 and $R_0 \propto N^{1/3}$ to obtain

$$R_g^2 \propto N^{2/3} f^{-2/5} \tag{3}$$

The upper panel of Figure 6 shows the simulation results for the radius of gyration $\langle R_g^2 \rangle$ of the swollen SCNPs as a function
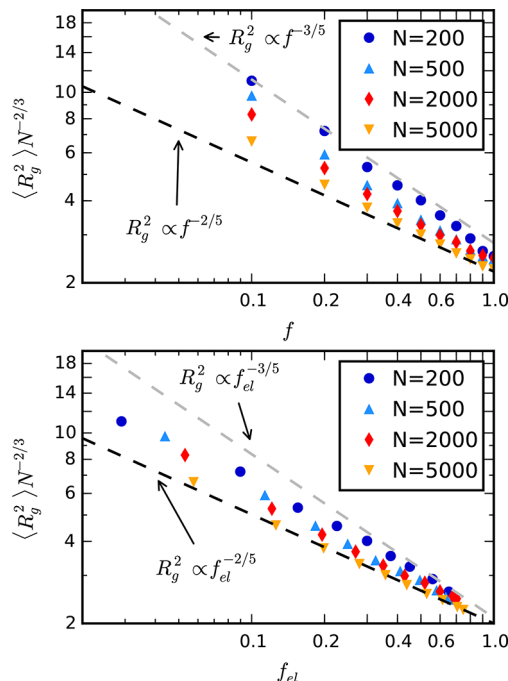

Figure 6. Ensemble average radius of gyration of SCNPs cross-linked under poor solvent conditions as a function of the cross-linking density (upper panel) and density of elastically active cross-links (lower panel), both compared to the prediction $\langle R_g^2 \rangle \propto f^{-2/5}$ from Flory−Rehner theory. A function $\langle R_g^2 \rangle \propto f^{-3/5}$ is shown for comparison. With growing N, the exponent approaches the value predicted by the Flory−Rehner ansatz. Using f_{el} as the relevant variable, long chains with $N = 5000$ are described well by the Flory−Rehner prediction.

of f. $\langle R_g^2 \rangle$ has been rescaled by $N^{-2/3}$ as suggested by eq 3. The results show a power law behavior $\langle R_g^2 \rangle \propto f^\alpha$, but a uniform decay with the same exponent across the different chain lengths cannot be observed with increasing number of cross-links. In fact, all observed exponents are smaller; i.e., $\langle R_g^2 \rangle$ decays faster than predicted by the Flory−Rehner theory. However, a trend of the exponents coming closer to the predicted value of $\alpha = -2/5$ with increasing chain length is clearly visible. In the lower panel of Figure 6 the same data are plotted as a function of the density of elastically active cross-links f_{el} instead of the total cross-linking density f. This number can be calculated as

$$f = \frac{4 N_{act}}{N} \rightarrow f_{el} = \frac{4(N_{act} - \langle N_{loop} \rangle)}{N}$$

where $\langle N_{loop} \rangle$ is average the number of links that only form dangling loops (Figure 7). N_{loop} was determined for each structure by iteratively traversing along the cross-linked precursor chain and deleting loops that return to their origin with no cross-links in between, as illustrated by the gray lines in Figure 7. Once this process has converged, the total number of loops deleted during the iteration corresponds to N_{loop}. With this correction the data points for the longest chain with $N = 5000$ almost perfectly follow the prediction by the Flory−
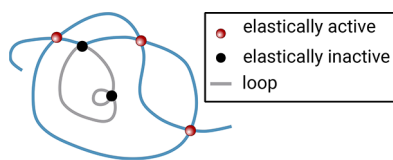
Figure 7. Cross-linkers which only forming loops do not elastically contribute to the network structure. When analyzing the scaling of the radius of gyration with the cross-linking density in terms of the Flory−Rehner theory (Figure 6) this should be taken into account.

Rehner theory, indicating that SCNPs formed from long precursor chains in poor solvent have network-like properties. Nevertheless, the results for shorter chains are still only moderately well described.

3.3. Flory-Type Mean-Field Theory. It was shown in section 3.2 that SCNPs formed under poor solvent conditions can be understood as polymer networks in the limit of long precursor chain lengths. In this section we aim at providing a theoretical description, which is more generally applicable. We begin the discussion with the regime of low cross-linking densities and short precursor chains, where the SCNPs do not have the characteristics of a network, as shown in section 3.1. We are going to show that a Flory-type mean-field approach can be used to describe the SCNPs in this regime. We then present a scaling argument to connect the two regimes of network-like and non-network-like topologies.

In the Flory−Rehner model employed in section 3.2 the elasticity is assumed to be homogeneously distributed among all elastically active strands. Effects of the details of the connectivity are not taken into account. The theoretical treatment can be improved by considering the true topology of the cross-linked structure in the framework of a mean-field model. Within the generalized Gaussian structure model for ideal polymers, repeat units of a polymer are assumed to be connected by harmonic spring potentials.[31,32] The overall potential energy of such a structure can then be written as

$$U(\{\vec{R}_i\}) = \frac{k_B T}{2\langle b^2 \rangle} \sum_{j,k} \vec{R}_j A_{jk} \vec{R}_k$$

where $\{\vec{R}_i\}$ are the coordinates of all monomers and A is the connectivity matrix, which is also known as the (generalized) Rouse matrix in polymer science.[33] For the ideal model without excluded volume, the average radius of gyration can then be rigorously calculated and is determined only by the eigenvalues λ of the connectivity matri and the average bond length $\langle b^2 \rangle$[32,34,35]

$$R_0{}^2 = \frac{\langle b^2 \rangle}{N} \sum_{\langle i \rangle} \frac{1}{\lambda_i}$$

(4)

where the notation $\langle i \rangle$ indicates that the zero eigenvalue representing the center of mass mode is excluded. For linear chains eq 4 leads to the known relation $R_0{}^2 \propto N$. For polymer networks $R_0{}^2$ is a rather abstract property because a network of ideal chains collapses to a size determined by the strand length $R_0{}^2 \propto N_S$, independent of the total number N of monomers. This statement for networks of ideal chains can be derived analytically,[32] and Figure 8 shows that it is indeed true for our simulations in the regime of high f, where SCNPs become network-like. On the other hand, for low f and short precursor chains R_0 depends on the random topology, and no simple relation between R_0, N, and f exists.
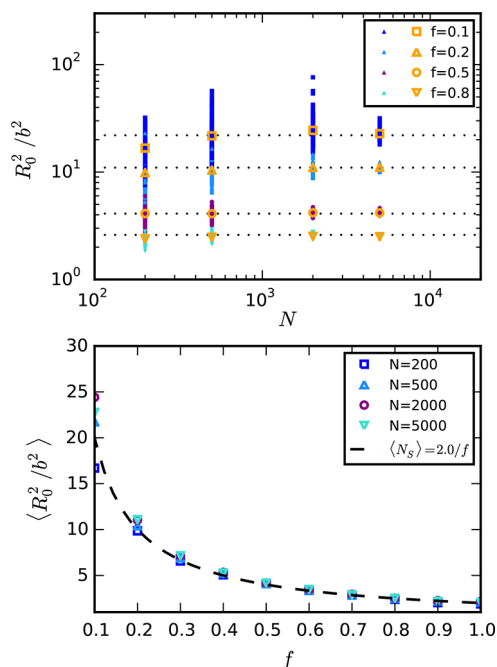

Figure 8. Ideal radius of gyration $R_0{}^2$ as calculated from eq 4 for SCNPs cross-linked under poor solvent conditions as a function of N (upper panel) and f (lower panel). The small symbols represent results from all random realizations, while the larger symbols are the averages $\langle R_0{}^2 \rangle$. For sufficiently large f, where SCNPs become network-like, there is no dependence of $R_0{}^2$ on N and hardly any scattering of the data.

In the spirit of the Flory theory for excluded volume chains, we now describe the average radius of gyration of the SCNPs with excluded volume by balancing the elastic contribution based on stretching of ideal chains, with a mean-field excluded volume term in the free energy. As shown in section 3.1, small chains at low cross-linking densities tend to form open fluffy structures instead of compact networks, even after cross-linking under poor solvent conditions. We assume in this case that there exists a characteristic elastic strand of g monomers which crosses the molecule and thus defines its spatial extension. In total, an average of N/g strands have to be deformed simultaneously when the molecule swells due to excluded volume. Then, the Flory-type free energy is given by

$$\frac{F(R_g)}{k_B T} = a \frac{N}{g} \frac{R_g{}^2}{R_0{}^2} + \nu \frac{N^2}{R_g{}^3} = a' N \frac{R_g{}^2}{R_0{}^4} + \nu \frac{N^2}{R_g{}^3}$$

(5)

The numerical prefactors a and a' account for the fact that we have used the radius of gyration to measure the extension of the molecule, and in the second step in eq 5 the relation $R_0{}^2 \propto g$ has been used because of the Gaussian conformations in the absence of excluded volume. This approach has previously been employed for branched polymers,[36−38] where the elasticity is also essentially defined by a characteristic strand crossing the molecule. In contrast, the elasticity of a polymer network is prescribed by a strand connecting two cross-linking points. Minimizing eq 5 with respect to the radius yields the equilibrium radius of gyration

$$R_g{}^2 = \left(\frac{3}{2} \frac{\nu}{a'} \right)^{2/5} N^{2/5} R_0{}^{8/5}$$

(6)

E

Equation 6 provides a prediction for the radius of gyration of every single simulated structure instead of only the ensemble average $\langle R_g^2 \rangle$, since the ideal radius R_0^2 can be calculated for every structure individually using eq 4. Note that the thus-derived formula reproduces the Flory exponent for linear chains, if $R_0 \propto N^{1/2}$ is substituted. As suggested by eq 6, Figure 9 shows R_g^2 as obtained from the simulations for all different cross-linking densities and chain lengths as a function of $N^{2/5}R_0^{8/5}$ with R_0^2 given by eq 4.
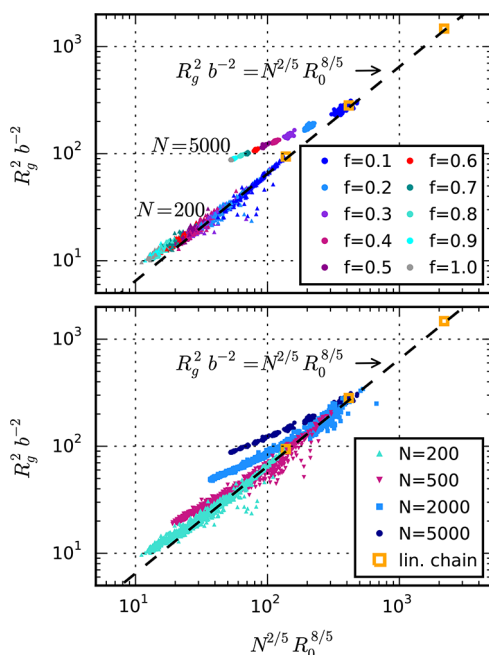

Figure 9. Radius of gyration of SCNP cross-linked under poor solvent conditions as a function of $N^{2/5}R_0^{8/5}$. The upper plot shows data for two different chain lengths, with the color code indicating the cross-linking density f. In the bottom plot the data for all simulated chain lengths are compared. The dashed line indicates the prediction by eq 6. Results for linear chains are displayed for comparison. The prediction works well for SCNP obtained from short chains and at low f, where SCNPs tend to have an open fluffy structure.

Equation 6 was derived for SCNPs with open fluffy strucutres by making the assumption that a characteristic strand length g defines the extension of the molecule. This assumption breaks down in particular once the cross-linked structure has the characteristics of a polymer network, because here the characteristic length is defined by a network strand $N_S \propto f^{-1}$ and not by the overall size of the structure. Accordingly, the data as shown in Figure 9 follow the prediction of eq 6 only for low cross-linking densities and particularly well for $N = 200$. This is consistent with the observation from section 3.1, where it was shown that the short precursor chains tend not to form compact networks.

Thus, we observe two limiting cases: fluffy, rather open structures, which are well described by the elasticity of threads traversing the whole molecule, and compact networks which follow the Flory–Rehner prediction. Both cases are separated by varying chain length and cross-link density. In the following we employ a scaling argument to connect the two cases and determine what is the prerequisite for a single polymer chain to form a compact network after cross-linking under poor solvent conditions. Prior to cross-linking the polymer is in a globular

state with volume $R_{glob}^3 \propto V = \nu_0 N$. In order for the structure to form a compact network after cross-linking, an average network strand should thus have a characteristic extension $R_{str} \lesssim R_{glob}$ smaller than that of the globule. Remembering that the ideal radius of gyration of a compact network is precisely that of a network strand, $R_0 = R_{str}$, this leaves us with the criterion

$$R_0 \lesssim (\nu_0 N)^{1/3}$$

for a compact network structure to be obtained. Using this argument, we assume the radius of gyration to be described by

$$R_g^2 = R_{ref}^2 \zeta(R_0/N^{1/3}) \tag{7}$$

with the reference radius R_{ref}^2 defined by eq 6 and a scaling function

$$\zeta(x) = \begin{cases} x^0 & x > x_c \\ x^m & x < x_c \end{cases}$$

where x_c is some characteristic, but *a priori* unknown crossover value. Large values of the scaling variable $x = R_0/N^{1/3}$ correspond to the open, branched structure, while small values of x correspond to compact networks. For large enough $R_0/N^{1/3}$ the functional form $\zeta(x) = x^0$ means that R_g^2 is described by eq 6. The exponent m is determined by the requirement that for low values of $R_0/N^{1/3}$ the polymeric object has the properties of a compact network and must stay globular; thus $R_g^2 \propto N^{2/3}$. This leads to $m = -4/5$. Inserting m back into the equation, we finally obtain

$$R_g^2(x) \propto \begin{cases} N^{2/5}R_0^{8/5} & x > x_c \\ N^{2/3}R_0^{4/5} \propto N^{2/3}f^{-2/5} & x < x_c \end{cases}$$

meaning that in the limit of small $R_0/N^{1/3}$ the result coincides with the Flory–Rehner theory, since in the network regime $R_0^2 \propto N_S \propto f^{-1}$ (compare section 3.2 and Figure 8).

In Figure 10 the radius of gyration is plotted as a function of $x = R_0/N^{1/3}$ and rescaled by $N^{2/5}R_0^{8/5}$, as suggested by eq 7. In both limits the simulation results follow the predictions. For very low values of the variable $R_0/N^{1/3}$ an exponent of $m \approx -4/5$ describes the data well. This is the regime in which the SCNP has the properies of a compact network, and the
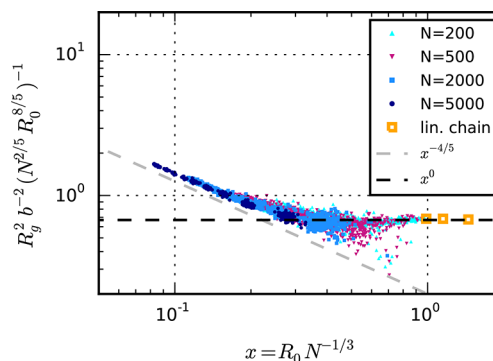

Figure 10. Radius of gyration of SCNPs cross-linked in poor solvent as a function of the scaling variable $x = R_0/N^{1/3}$ and rescaled according to eq 7. The data are the same as shown in Figure 9. In the limit of low x, SCNPs have network-like properties and are described by well by the Flory–Rehner theory, which leads to the exponent of $-4/5$ in the plot. For large enough x the SCNPs are open structures and follow eq 6, as indicated by the horizontal line.

Flory–Rehner theory offers a good description of the swelling behavior. After a crossover at $R_0/N^{1/3} \approx 0.5 = x_c$ the SCNPs are rather open structures, and the radius of gyration is described by eq 6, as indicated by the horizontal alignment of the data points in Figure 10. Note that the theory also describes consistently the radius of gyration of linear chains, corresponding to the limit of a cross-linking density of $f = 0$.

The scaling analysis should allow in principle for an experimental estimation of the cross-linking density required for forming compact SCNPs at given N. The horizontal line for non-network structures in Figure 10 could be estimated by measuring R_g^2 of linear chains, for which $R_0^2 \propto N$ is known. On the other side, $R_0^2 \propto 1/f$ holds in the network-forming regime, allowing for an estimate of the line with slope $-4/5$ based on measurements with sufficiently high N and f. Extrapolating both lines to find their intersection would then give an estimate for the crossover x_c, which translates to a cross-linking density when approaching from high f according to $x = R_0 N^{-1/3} \propto f^{-1/2} N^{-1/3}$. Thus, the crossover condition to compact SCNPs reads

$$f_c \propto N^{-2/3}$$

The theoretical argument developed here can also be applied to SCNPs cross-linked under good solvent conditions. Since in this case the SCNPs do not form network-like structures, we can expect them to have a characteristic ratio $R_0/N^{1/3}$ above the crossover. This is indeed the case, as Figure 11 shows.
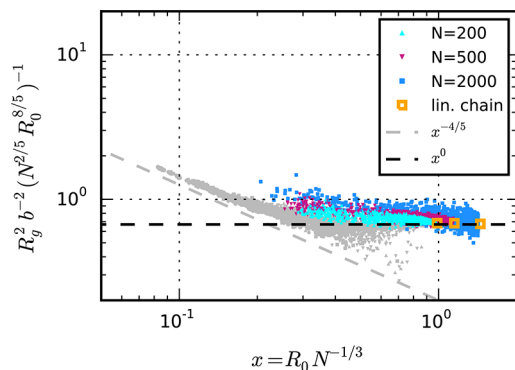

Figure 11. Radius of gyration of SCNPs cross-linked in good solvent as a function of the scaling variable $x = R_0 N^{-1/3}$ and rescaled according to eq 7. The results from cross-linking in poor solvent are shown as gray data points in the background for comparison. The theory can consistently describe both cases, but a small offset to higher R_g^2 is visible when cross-linking in good solvent. This effect may be caused by the formation of concatenated ring structures, which provide additional effective cross-links.

However, a small, but clearly visible offset toward larger values of the rescaled radius of gyration R_g^2/R_{ref}^2 is present between the data obtained from good and poor solvent. We hypothesize that this can be attributed to the formation of concatenated ring structures, which are more likely to form when cross-linking from a collapsed globule, as compared to cross-linking in good solvent. Figure 12 displays a simulation snapshot of such a structure. Concatenations provide additional effective cross-links leading to a reduced R_g^2 and are not accounted for by the theory presented here. This topological effect may also be the cause for the relatively broad scattering of data points in Figure 10 around the crossover point. Further studies of this matter will be subject of future investigations.
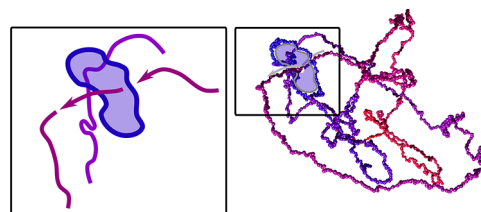

Figure 12. Simulation snapshot showing at least one concatenated ring structure along with an abstracted and enlarged sketch of the relevant region. Such topological effects are not captured in the theory presented here. The snapshot is taken from a configuration with $N = 2000$ and a cross-linking density of $f = 0.1$.

3.4. Distribution of Contour Distances. To obtain a more detailed understanding of the network structure, we analyze the distribution of contour distances, $P(s)$, between cross-linking points. The contour distance s is measured as the topological distance between monomers along the original precursor chain. This distribution is displayed in Figure 13 for
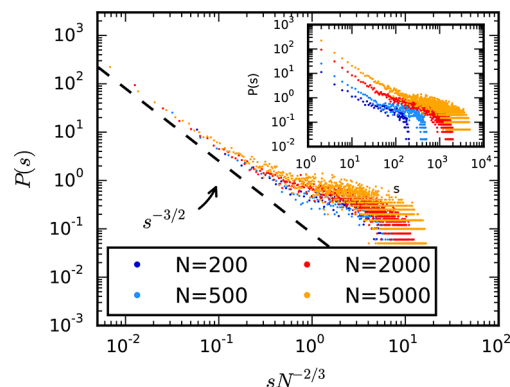

Figure 13. Distribution of contour distances as a function of $s/N^{2/3}$ for cross-linking in poor solvent with cross-linking density $f = 1.0$. The distribution follows the statistics of intrachain contacts in a collapsed globule with a characteristic shoulder developing at $s_c \propto N^{2/3}$. The inset shows the same data without rescaling of the contour distance.

all simulated chain lengths at degree of cross-linking $f = 1.0$ for the case of poor solvent. The distributions follow a power law decay $P(s) \propto s^{-3/2}$ for low values of s, followed by a shoulder for high s. This behavior agrees well with the observations by other authors.[24] We want to point out here that the origin of this particular shape of $P(s)$ is to be found simply in the statistics of linear chain segments within a collapsed globule.[39] To show this, we have plotted the distribution $P(s)$ in Figure 13 such that we rescale the contour length with $N^{2/3}$. Thus, the crossover point between power law decay and plateau can be scaled on top of each other for the different chain lengths. We briefly outline the argument leading to this scale factor,[39] which is similar in spirit to the scaling argument used above in the analysis of R_g^2. A chain segment of length s within a globule is in a melt-like environment and thus follows Gaussian statistics. The return probability thus scales with the length of the segment as $\propto s^{-3/2}$. This scaling breaks down once the average size of the Gaussian segment, $R_{seg} \propto s^{1/2}$, reaches the size of the globule $R_{glob} \propto N^{1/3}$, where the chain sequence is reflected back into the globule. The characteristic segment length s_c is thus given by $s_c \propto N^{2/3}$.

The fact that the distribution of contour distances between cross-linking points follows precisely the rationale for the

unlinked globule simply means that the bond structure represents a snapshot of the intrachain contact distribution within a unlinked structure. We finish the discussion by noting that this is in contrast to the case of cross-linking under good solvent conditions. There, the distribution of contour distances decays as $s^{-\Phi}$ with an exponent of $\Phi \approx 1.5$ (data not shown). The unlinked chain in good solvent, on the other hand, shows a decay of intrachain contacts with $\Phi \approx 2.1$, as first derived by Des Cloizeaux.[40,41]

4. SUMMARY AND CONCLUSIONS

We have studied the static properties and swelling behavior of single-chain polymer nanoparticles by means of generic Monte Carlo simulations and theoretical analysis. Nanoparticles were constructed using two different simulation protocols as well as precursor chain lengths in the range $N = 200-5000$. In the first approach, the polymers were cross-linked from a collapsed, globular conformation under poor solvent conditions. In the second approach the cross-linking was carried out in good solvent. For both cases we studied a broad range of cross-linking densities f. In agreement with results from other groups, we find that cross-linking in good solvent does not result in the formation of compact structures, even for high cross-linking densities. Opposed to this, cross-linking under poor solvent conditions can lead to compact structures with properties of a polymer network. We have examined the conditions required for this by means of mean-field theories and scaling arguments. The swelling behavior of nanoparticles with the longest simulated chain length ($N = 5000$) can be described well within the Flory−Rehner theory for polymer networks in the complete range of cross-linking densities considered. With decreasing chain length and cross-linking density, this approach fails, and the nanoparticles in this regime are appropriately described by a Flory-type mean-field theory, which has been used previously for branched polymers and is based on the analysis of the connectivity matrix. Using a scaling approach, we have shown that the relevant variable that separates the two limiting cases is the ratio $x = R_0/N^{1/3}$, in which R_0 is the radius of gyration of an ideal polymer without excluded volume, but with the same bond structure as the original cross-linked nanoparticle. The crossover from the compact network to an open fluffy structure can also be characterized by a condition for the number of cross-links in the precursor chains as $f_c \propto N^{-2/3}$. The thus-derived theoretical framework describes consistently single-chain nanoparticles obtained under good and poor solvent conditions. Small deviations from the theory can likely be attributed to the formation of entanglements due to concatenated ring structures. A closer investigation of this topological effect might be the subject of future studies. An analysis of the distribution of distances s between cross-linking points along the chain contour has shown that chain segments follow Gaussian statistics within the globule and that cross-linking from a collapsed globule preserves the spatial correlation of monomer distances.

AUTHOR INFORMATION

Corresponding Author

*E-mail: sommer@ipfdd.de (J.-U.S.).

ORCID

Hauke Rabbel: 0000-0002-9387-3999
Jens-Uwe Sommer: 0000-0001-8239-3570

Notes

The authors declare no competing financial interest.

REFERENCES

(1) Mecerreyes, D.; Lee, V.; Hawker, C. J.; Hedrick, J. L.; Wursch, A.; Volksen, W.; Magbitang, T.; Huang, E.; Miller, R. D. Novel Approach to Functionalized Nanoparticles: Self-crosslinking of Macromolecules in Ultradilute Solution. *Adv. Mater.* **2001**, *13*, 204−208.

(2) Hanlon, A. M.; Lyon, C. K.; Berda, E. B. What Is Next in Single-Chain Nanoparticles? *Macromolecules* **2016**, *49*, 2−14.

(3) Lyon, C. K.; Prasher, A.; Hanlon, A. M.; Tuten, B. T.; Tooley, C. A.; Frank, P. G.; Berda, E. B. A Brief User's Guide to Single-Chain Nanoparticles. *Polym. Chem.* **2015**, *6*, 181−197.

(4) Altintas, O.; Barner-Kowollik, C. Single-Chain Folding of Synthetic Polymers: A Critical Update. *Macromol. Rapid Commun.* **2016**, *37*, 29−46.

(5) Pomposo, J. A. Bioinspired Single-Chain Polymer Nanoparticles. *Polym. Int.* **2014**, *63*, 589−592.

(6) Gonzalez-Burgos, M.; Latorre-Sanchez, A.; Pomposo, J. A. Advances in Single Chain Technology. *Chem. Soc. Rev.* **2015**, *44*, 6122−6142.

(7) Hamilton, S. K.; Harth, E. Molecular Dendritic Transporter Nanoparticle Vectors Provide Efficient Intracellular Delivery of Peptides. *ACS Nano* **2009**, *3*, 402−410.

(8) Sanchez-Sanchez, A.; Akbari, S.; Moreno, A. J.; Lo Verso, F.; Arbe, A.; Colmenero, J.; Pomposo, J. A. Design and Preparation of Single-Chain Nanocarriers Mimicking Disordered Proteins for Combined Delivery of Dermal Bioactive Cargos. *Macromol. Rapid Commun.* **2013**, *34*, 1681−1686.

(9) Perez-Baena, I.; Barroso-Bujans, F.; Gasser, U.; Arbe, A.; Moreno, A. J.; Colmenero, J.; Pomposo, J. A. Endowing Single-Chain Polymer Nanoparticles with Enzyme-Mimetic Activity. *ACS Macro Lett.* **2013**, *2*, 775−779.

(10) Terashima, T.; Mes, T.; De Greef, T. F. A.; Gillissen, M. A. J.; Besenius, P.; Palmans, A. R. A.; Meijer, E. W. Single-Chain Folding of Polymers for Catalytic Systems in Water. *J. Am. Chem. Soc.* **2011**, *133*, 4742−4745.

(11) Artar, M.; Terashima, T.; Sawamoto, M.; Meijer, E. W.; Palmans, A. R. A. Understanding the Catalytic Activity of Single-Chain Polymeric Nanoparticles in Water. *J. Polym. Sci., Part A: Polym. Chem.* **2014**, *52*, 12−20.

(12) Mackay, M. E.; Dao, T. T.; Tuteja, A.; Ho, D. L.; van Horn, B.; Kim, H.-C.; Hawker, C. J. Nanoscale Effects Leading to Non-Einstein-Like Decrease in Viscosity. *Nat. Mater.* **2003**, *2*, 762−766.

(13) Harth, E.; Horn, B. V.; Lee, V. Y.; Germack, D. S.; Gonzales, C. P.; Miller, R. D.; Hawker, C. J. A Facile Approach to Architecturally Defined Nanoparticles via Intramolecular Chain Collapse. *J. Am. Chem. Soc.* **2002**, *124*, 8653−8660.

(14) Altintas, O.; Willenbacher, J.; Wuest, K. N. R.; Oehlenschlaeger, K. K.; Krolla-Sidenstein, P.; Gliemann, H.; Barner-Kowollik, C. A Mild and Efficient Approach to Functional Single-Chain Polymeric Nanoparticles via Photoinduced Diels-Alder Ligation. *Macromolecules* **2013**, *46*, 8092−8101.

(15) Frank, P. G.; Tuten, B. T.; Prasher, A.; Chao, D.; Berda, E. B. Intra-Chain Photodimerization of Pendant Anthracene Units as an Efficient Route to Single-Chain Nanoparticle Fabrication. *Macromol. Rapid Commun.* **2014**, *35*, 249−253.

(16) He, J.; Tremblay, L.; Lacelle, S.; Zhao, Y. Preparation of Polymer Single Chain Nanoparticles Using Intramolecular Photo-dimerization of Coumarin. *Soft Matter* **2011**, *7*, 2380−2386.

(17) Sanchez-Sanchez, A.; Perez-Baena, I.; Pomposo, J. A. Advances in Click Chemistry for Single-Chain Nanoparticle Construction. *Molecules* **2013**, *18*, 3339−3355.

(18) Murray, B. S.; Fulton, D. A. Dynamic Covalent Single-Chain Polymer Nanoparticles. *Macromolecules* **2011**, *44*, 7242−7252.

(19) Mes, T.; Van Der Weegen, R.; Palmans, A. R. A.; Meijer, E. W. Single-Chain Polymeric Nanoparticles by Stepwise Folding. *Angew. Chem., Int. Ed.* **2011**, *50*, 5085−5089.

(20) Foster, E. J.; Berda, E. B.; Meijer, E. W. Metastable Supramolecular Polymer Nanoparticles via Intramolecular Collapse of Single Polymer Chains. *J. Am. Chem. Soc.* **2009**, *131*, 6964−6966.

(21) Moreno, A. J.; Lo Verso, F.; Sanchez-Sanchez, A.; Arbe, A.; Colmenero, J.; Pomposo, J. A. Advantages of Orthogonal Folding of Single Polymer Chains to Soft Nanoparticles. *Macromolecules* **2013**, *46*, 9748−9759.

(22) Lo Verso, F.; Pomposo, J. A.; Colmenero, J.; Moreno, A. J. Multi-Orthogonal Folding of Single Polymer Chains into Soft Nanoparticles. *Soft Matter* **2014**, *10*, 4813−4821.

(23) Perez-Baena, I.; Asenjo-Sanz, I.; Arbe, A.; Moreno, A. J.; Lo Verso, F.; Colmenero, J.; Pomposo, J. A. Efficient Route to Compact Single-Chain Nanoparticles: Photoactivated Synthesis via Thiol-yne Coupling Reaction. *Macromolecules* **2014**, *47*, 8270−8280.

(24) Lo Verso, F.; Pomposo, J. A.; Colmenero, J.; Moreno, A. J. Simulation Guided Design of Globular Single-Chain Nanoparticles by Tuning the Solvent Quality. *Soft Matter* **2015**, *11*, 1369−1375.

(25) Pomposo, J. A.; Perez-Baena, I.; Lo Verso, F.; Moreno, A. J.; Arbe, A.; Colmenero, J. How Far Are Single-Chain Polymer Nanoparticles in Solution From the Globular State? *ACS Macro Lett.* **2014**, *3*, 767−772.

(26) Chao, D.; Jia, X.; Tuten, B.; Wang, C.; Berda, E. B. Controlled Folding of a Novel Electroactive Polyolefin via Multiple Sequential Orthogonal Intra-Chain Interactions. *Chem. Commun. (Cambridge, U. K.)* **2013**, *49*, 4178−4180.

(27) Carmesin, I.; Kremer, K. The Bond Fluctuation Method: A New Effective Algorithm for the Dynamics of Polymers in All Spatial Dimensions. *Macromolecules* **1988**, *21*, 2819−2823.

(28) Deutsch, H. P.; Binder, K. Interdiffusion and Self-Diffusion in Polymer Mixtures: A Monte Carlo Study. *J. Chem. Phys.* **1991**, *94*, 2294−2304.

(29) Jentzsch, C.; Werner, M.; Sommer, J.-U. Single Polymer Chains in Poor Solvent: Using the Bond Fluctuation Method with Explicit Solvent. *J. Chem. Phys.* **2013**, *138*, 094902.

(30) Wengenmayr, M.; Dockhorn, R.; Sommer, J.-U. Multicore Unimolecular Structure Formation in Single Dendritic-Linear Copolymers under Selective Solvent Conditions. *Macromolecules* **2016**, *49*, 9215−9227.

(31) Doi, M.; Edwards, S. F. *The Theory of Polymer Dynamics*; Oxford University Press: 1988.

(32) Sommer, J.-U.; Blumen, A. On the Statistics of Generalized Gaussian Structures: Collapse and Random External Fields. *J. Phys. A: Math. Gen.* **1995**, *28*, 6669−6674.

(33) Sommer, J.-U.; Schulz, M.; Trautenberg, H. L. Dynamical Properties of Randomly Cross-Linked Polymer Melts: A Monte Carlo Study. I. Diffusion Dynamics. *J. Chem. Phys.* **1993**, *98*, 7515−7520.

(34) Eichinger, B. Configurational Statistics of Gaussian Molecules. *Macromolecules* **1980**, *13*, 1−11.

(35) Kumar, A.; Biswas, P. Conformational Transitions in Semi-flexible Dendrimers Induced by Bond Orientations. *J. Chem. Phys.* **2012**, *137*, 124903.

(36) Boris, D.; Rubinstein, M. A Self-Consistent Mean Field Model of a Starburst Dendrimer: Dense Core vs Dense Shell. *Macromolecules* **1996**, *29*, 7251−7260.

(37) Kłos, J. S.; Sommer, J.-U. Properties of Dendrimers with Flexible Spacer-Chains: A Monte Carlo Study. *Macromolecules* **2009**, *42*, 4878−4886.

(38) Jurjiu, A.; Dockhorn, R.; Mironova, O.; Sommer, J.-U. Two Universality Classes for Random Hyperbranched Polymers. *Soft Matter* **2014**, *10*, 4935−4946.

(39) Lua, R.; Borovinskiy, A. L.; Grosberg, A. Y. Fractal And Statistical Properties of Large Compact Polymers: A Computational Study. *Polymer* **2004**, *45*, 717−731.

(40) Des Cloizeaux, J. Lagrangian Theory for a Self-Avoiding Random Chain. *Phys. Rev. A: At., Mol., Opt. Phys.* **1974**, *10*, 1665−1669.

(41) De Gennes, P. G. In *Scaling Concepts in Polymer Physics*; De Gennes, P. G. E., Ed.; Cornell University Press: 1979.